Thermophysics and Aeromechanics, *2015*, *Vol. 22*, *No. 4*

Control of turbulent boundary layer through air blowing due to external-flow resources

V.I. Kornilov, A.V. Boiko, and I.N. Kavun

Khristianovich Institute of Theoretical and Applied Mechanics SB RAS, *Novosibirsk*, *Russia*

E-mail: kornilov@itam.nsc.ru

(*Received August 29*, *2014*)

The possibility to control turbulent incompressible boundary layer using air blowing through a finely perforated wall presenting part of the streamlined flat-plate surface was examined. The control was exercised via an action on the state and characteristics of the near-wall flow exerted by controlled (through variation of external-pressure-flow velocity) blowing of air through an air intake installed on the idle side of the plate. A stable reduction of the local values of skin friction coefficient along the model, reaching 50 % at the end of the perforated area, has been demonstrated. The obtained experimental and calculated data are indicative of a possibility to model the process of turbulent-boundary-layer control by air blowing due to external-flow resources.

Key words: control, turbulent boundary layer, plate, intake, finely perforated surface, blowing, skin friction.

Introduction

To date, the aerodynamic shape and finish of aircraft surfaces have reached so high perfection that, in the nearest future, further progress in improving those characteristics can hardly be expected to enable a substantial reduction of aircraft frictional drag. Simultaneously, the energy efficiency problem [1] that has arisen due to the necessity of reducing the rate of fuel consumption per passenger-kilometer has become an increasingly vital problem. The latter implies that further progress in the development of transportation systems, including aircraft, is hardly possible without use of new energy-efficient methods to control the near-wall flows. That is why the enhancement of aircraft effectiveness due to reduced aircraft viscous drag is presently regarded as the most promising strategy for the next 10–20 years [2]. However, in the flow past aircraft components such as the aircraft fuselage or rocket body, in a broad range of Reynolds numbers the boundary layer is in turbulent state. That is why artificial means to control turbulent flows such as, in particular, gas blowing [3–8] through advanced finely perforated permeable surfaces seems to be ones offering a promising way toward friction-induced and net aerodynamic drag reduction and, hence, toward raising the aircraft aerodynamic efficiency. As a consequence, the latter offers a possibility to increase both the aircraft range and useful load, and to reduce the aircraft fuel and direct operational costs.

The present study is a generalization of our previous experiments on the use of a new method to control turbulent incompressible boundary layers on streamlined flat surfaces by air blowing through a hydraulically smooth, finely perforated wall due to outside (free) stream resources. The necessity to test the effectiveness of this method has arisen in connection with an unexpected result that was obtained by us at the previous stage of the study [9]. It was found that passive air flow through a perforated wall (without forced blowing) resulting from the natural drop of pressure between the barometric and static pressures in the wind-tunnel test section, enables more-than-30-% reduction of skin friction. Here, an increase in freestream velocity leads to natural growth of blowing intensity through the perforated surface and to a related reduction of skin friction. The latter offers a possibility to exert, in a similar way, control over turbulent boundary layers in earth-bound environment.

1. Instrumentation, experimental procedure, and experimental conditions

1.1. Experiment

The experiments were carried out in the T-324 subsonic low-turbulence wind tunnel of Khristianovich Institute of Theoretical and Applied Mechanics. The test section of the wind tunnel has dimensions 1×1×4 m. The experiments covered the range of undisturbed flow velocities U_∞ in the reference section 9 to 23 m/s; those values correspond to Reynolds numbers per one meter $\mathrm{Re}_1 = (0.60–1.53)\cdot 10^6\ \mathrm{m}^{-1}$.

The measurements were carried out on a flat-plate model prepared from D16T duralumin. The in-plan sizes of the model were 2204.5×993 mm, and its thickness was 6 mm. The model was installed horizontally in the wind-tunnel test section on guiding side rails. On the idle side of the plate, its leading and trailing parts were shaped as semiellipses with semi-axis ratio $b/a = 1 : 12$ (Fig. 1). The shape of the leading edge had rounding with radius $r = 0.4$ mm. Several 0.4-mm diameter static-pressure orifices were provided along the symmetry axis of the plate. The trailing part of the model was provided with an adjustable tail flap. The chord of the tail flap was 170 mm long. The flap spanned the entire width of the test section, and it was used to control the flow pattern in the vicinity of the leading edge. The distribution of pressure over the rest portion of the plate could be modified via an insignificant change of the guiding-rail elevation angle.

The design of the plate provided a possibility to install, flush with the main plate surface, a changeable finely perforated flat-plate sample insert having sufficiently large in-plan dimensions (420 × 250 mm); this allowed us to control the local flow quantities, namely, the mean velocity, skin friction, and velocity fluctuations, at rather large downstream distances x. The position of the beginning "b" and end "e" of the insert over the plate length was defined by the coordinates $\bar{x}_\mathrm{b} = x_\mathrm{b}/L = 0.486$ and $\bar{x}_\mathrm{e} = x_\mathrm{e}/L = 0.668$.

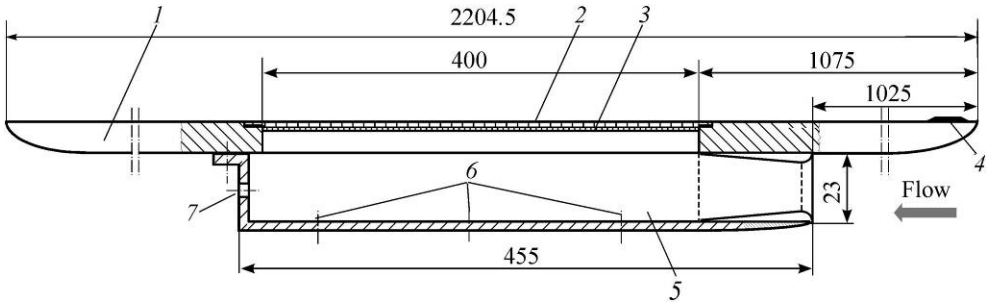

Fig.1. Schematic of the model.

1 — flat plate, *2* — finely perforated insert, *3* — filter, *4* — boundary-layer tripping device, *5* — air intake, *6* — pressure holes, *7* — adjustable airflow leafs.

The permeability of the plate material was characterized by the following parameters: porosity 17.1 %, areally mean diameter of staggered pores (holes) $D = 0.17$ mm, pore extension $\lambda = t/D = 6.47$ (here, $t = 1.1$ mm is the pore wall thickness). In the main test series, the ratio between the diameter of the pressure holes and the thickness of the initial (unmodified) boundary layer upstream of the perforated insert was 1/125. The values of the mentioned geometrical parameters were chosen based on the results of [10], those results indicating that the adopted configuration of the blowing holes was quite efficient (or, probably, even optimal) from the viewpoint of reducing the skin-friction coefficient C_f. It turned out that at porosities in excess of 23 %, the rate of the reduction of C_f substantially decreased. The results of previous studies [6, 11] have also demonstrated that, even at a relatively moderate porosity, one can obtain, due to air blowing, a friction reduction effect approaching, at $2C_b/C_{f0} = 4$, its maximum possible theoretical value [12].

In the course of an experiment, the freestream air entered an intake of rectangular cross section mounted on the lower (idle) side of the plate right under the perforated insert. Then, airflow moved from the intake, through an intermediate filter and a permeable wall, into the boundary layer. From the inner side, the leading part of the intake was a semi-airfoil whose shape could be represented by the formula

$$y = 30(0.2969\sqrt{\bar{x}} - 0.126\bar{x} - 0.3516\bar{x}^2 + 0.2843\bar{x}^3 - 0.1015\bar{x}^4),$$

where $\bar{x} = x/c$, and c is the chord of the semi-airfoil equal to 50 mm. From the outer side, the leading part of the air intake was a semi-ellipse whose axis ratio was 1 : 33.

Two considerations were used as the basis for the choice of this shape. First, we wanted to obtain a flow without flow separation at the entrance to the intake channel. Second, we wanted to generate an increased pressure in the latter channel providing a maximum rate of the airflow through the perforated surface. We, however, do not claim that the intake channel design in our study was an optimal one. In particular, the trailing part of the intake was an ordinary flat wall installed normally to the flow with the connections of the horizontal and vertical walls being not smooth; as a result, a 3D flow with longitudinally developing vortices could form in the vicinity of the conjunction lines [13]. Moreover, in the downstream region of the intake forebody, from the side of the perforated wall, there was a small construction ledge.

The flat-plate boundary layer was artificially tripped by a 30-mm wide sandpaper strip located in the region with the maximum pressure change (region in the vicinity of the leading edge of the plate). The grain size of the sandpaper was $h = 0.8$ mm. The choice of the indicated parameters of the tripping device was motivated by the necessity to obtain a developed turbulent flow over the plate length at a minimum flow velocity of 9 m/s. Simultaneously, at increased flow velocities and, in particular, upon the attainment of working flow velocity $U_\infty = 21$ m/s, such a tripping device led to artificial enhancement of boundary-layer thickness in comparison with the canonical value.

The freestream dynamic-pressure velocity q_∞ was determined as the difference between the total pressure P_0 and the static pressure P_∞ measured with the help of a Prandtl tube installed in the freestream and registered with a DISA inclined alcohol micromanometer. In addition, the freestream dynamic pressure was evaluated as the pressure difference $P_{0sc} - P_{ts}$, where P_{0sc} is the stagnation pressure in the wind-tunnel settling chamber and P_{ts} is the static pressure in the wind-tunnel test section.

The main measurement series was performed using a completely automated (x, y) traversing gear. Displacements of the moving part of the traversing gear over boundary-layer height y were made according to a prescribed procedure implying the choice of a desired

scanning step value (down to 1 μm) and the collection of desired characteristics on the mean-velocity field and turbulence characteristics. Both the acquisition and processing of registered data were conducted in real time, and the data obtained were analyzed using utilities developed around the MatLab software.

The instantaneous flow velocity u at the examined point of the shear flow field was measured with the help of a set of DANTEC 55M0 single-component constant-temperature hot-wire anemometer. The experimental arrangement involved a 55M10 hot-wire bridge with a 55D10 linearizer connected to the bridge output. The collection of measured data was organized as follows. The signal from the linearizer output was fed into an E-440 L-CARD multichannel high-frequency 14-bit external unit intended for digitization of input analog signals. From the output of the unit, the digitized data were fed, through an USB port, into a personal computer. At each measured point of the velocity field, data were collected during a 15-s period at 10-kHz sampling rate. The constant component of the signal corresponding to the mean flow velocity in boundary layer was measured by a 55D31 digital dc voltmeter. Visual inspection of the waveform of the turbulent signal was carried out using an C1-73 oscilloscope.

As a primary measurement transducer, a miniature hot-wire probe known in the literature as the boundary-layer probe was used. The sensing element of the probe was a 5-μm diameter tungsten wire of length 1.2 mm. The sensor element operated in constant-temperature mode with 1.7 overheat. During measurements, the probe body was oriented at an angle of 5° with respect to the velocity vector of the freestream. While the probe moved toward the wall (the negative direction of the y-axis), it finally touched the plate surface with the tips of the prongs. The tips of the prongs in the used hot-wire probe were "patches" about 86 μm in diameter. At the moment of touch, which was identified from the establishment of an electric contact with the wall, the distance from the surface to the middle of the wire diameter was fixed, equal to 43 μm. As the probe moved away from the wall (the positive direction of the y-axis), it detached from the surface after elimination of natural backlash. False (within the limits of the backlash) readings were discarded. In this procedure, the estimated inaccuracy was ±2 μm.

The flow temperature in the wind-tunnel test section was measured by a J-type thermocouple installed in freestream. The signal generated by the thermocouple was registered by an Agilent multimeter (model 34970A).

Like it was made in the previous study [6], the local skin-friction coefficient C_f was considered as the main determining quantity in evaluation of the effectiveness of the proposed control method for turbulent boundary layer. Substantiation of the procedure for determining the value of C_f in non-canonical turbulent flow with blowing was given elsewhere [14]. Note that, in the latter case, in addition to routine calibration of the hot-wire probe in the freestream, also thorough calibration of this probe at various locations over wall-normal coordinate y at different values of freestream velocity U_∞ around the regime value of this velocity was performed. Such additional calibration allowed us to take into account the effect of wall cooling on hot-wire anemometer readings to obtain an adequate description of flow velocity distribution in the near-wall portion of the velocity profile and, as a consequence, to gain a possibility to determine the value of C_f not only by the logarithmic portion of the velocity profile (if any) but, also, using measurements in the viscous sublayer.

The method for determining skin friction by the above procedure was tested for adequacy by comparing data obtained for conditions without air blowing with data that were obtained by direct measurements [15]. It is a well-known fact that, within the locally equilibrium model, the friction stress $\overline{u'v'}$ can be represented in terms of turbulent viscosity ν_t as follows:

$$-\overline{u'v'} = \nu_t (du/dy). \tag{1}$$

Here, $\nu_t = \kappa v_* y$, $v_* = (\tau_w / \rho)^{1/2}$ is the friction velocity, and κ is the Kármán constant. The values of $\overline{u'v'}$ were calculated on the condition that $y^+ = y v_* / \nu < 30$ ($y/\delta_{0.99} = 0.1$), that is, in the constant-friction stress layer. The estimates thus obtained have shown that the maximum difference between the experimental values of $\overline{u'v'}$, which was obtained in the present study by treating the data of [15], never exceeded 6 %.

The random error in determining the main characteristics such as, for instance, the displacement thickness ($\sigma\delta^*$), the momentum thickness ($\sigma\delta^{**}$), and the local skin-friction coefficient (σC_f), was evaluated using eight measured velocity profiles in the boundary layer without blowing; this error amounted, respectively, to $\pm 3\sigma\delta^* = 0.90$ %, $\pm 3\sigma\delta^{**} = 0.84$ %, and $\pm 3\sigma C_f = 0.51$ %. We would like to emphasize here that the above values are not the overall relative errors, but their random values which, strictly speaking, reflected the functioning stability of the measuring equipment used. Actually, the experiment might involve other types of inaccuracies (for instance, systematic errors) whose presence not always can be revealed. That is why the actual inaccuracy in determining the integral quantities δ^*, δ^{**}, and C_f may appear somewhat different. A subsequent analysis has shown that this inaccuracy was indeed higher (see Section 2.2.2).

1.2. Calculation

The problem about the flow past a plate with an installed intake was solved numerically using the ANSYS Fluent software. In solving the problem, Reynolds-averaged two-dimensional Navier–Stokes equations for viscous incompressible liquid were used. The equation system was closed by the Launder–Spalding k-ε two-parametric differential model of turbulence [16]. The solution was constructed in stationary statement by the relaxation method. In calculating the mean flow and turbulence quantities, counterflow schemes of the second and first approximation order were used. The computational domain was a rectangle whose upper and lower boundaries were the ceiling and the floor of the wind-tunnel test section, and the inlet and outlet boundaries were located, respectively, at distances 2000 and 1000 mm from the leading and trailing edge of the plate. At the inlet boundary, the magnitude of freestream velocity was a specified parameter, the turbulence intensity was assumed small (of order 0.05 %), and the molecular-to-turbulent viscosity ratio $\mu_\infty / \mu_{t\infty}$ was chosen equal to unity. The configuration of the calculation model comprised the following components: a plate area located in the upstream region of a perforated insert; the perforated insert itself, whose lower surface was provided with an underlying permeable support (filter); a pressure chamber located under the initial and perforated plate areas, the air intake, and the tail part of the plate. On the whole, the geometry of the calculation model was identical to the geometry of the experimental model except for the lower (idle) surface, where, unlike in the experiment, a graded junction between the pressure chamber and the trailing edge of the plate was set.

For simplification of problem, the perforated wall was replaced with a surface with 400 spanwise slits uniformly distributed in the direction of the coordinate x at 1-mm step. Each slit was 0.171 mm wide, and the intervals between the slits were 0.829 mm. Over width, each slit comprised ten calculation cells, and each interval in between the slits comprised 25 cells. All in all, the whole computational domain contained 5.5 million rectangular cells. This statement of the problem allowed us to study the flow in the vicinity of a perforated plate with the same permeability (17.1 %) like that implemented in the experiment. For reaching a sufficient accuracy, clustering of the computational grid along the wall-normal coordinate y was used so that to ensure the value $y^+ \sim 0.2$. As a result, the turbulent boundary layer on the plate could be resolved together with the laminar sublayer.

As was noted above, for improving the uniformity of the gas blowing through the perforated surface, a special filter was used in the experiments. In the numerical calculation, the filter was treated as a porous material, and the flow through this material was modeled as a laminar one using the Darcy law:

$$\text{grad } p = -k\,\mu\,\vec{\mathbf{v}}_{\text{ref}},$$

where grad p is the gradient of pressure along the streamline, $\vec{\mathbf{v}}_{\text{ref}}$ is the volume velocity vector in the porous region, μ is the dynamic viscosity of air, and k is the hydraulic drag coefficient of the pores. The volume velocity was defined as

$$\vec{\mathbf{v}}_{\text{ref}} = \gamma\vec{\mathbf{v}},$$

with $\vec{\mathbf{v}}$ being the mean velocity vector of the flow in the porous channels, and γ, the porosity factor of the material, that is, the ratio between the air-filled space in the porous material and the total volume of this material. In the performed calculations, values $k = 3.07\cdot10^{11}$ m^{-2} and $\gamma = 0.5$ were adopted.

2. Results and discussion

2.1. Boundary layer in the absence of intake airflow

At the initial stage of our experiments, we analyzed the state of the shear flow on the flat plate in the absence of intake airflow. In the latter case, the intake inlet was plugged with a special profiled closing cap that ensured the absence of flow separation in the region around the air intake.

For technical reasons, no pressure holes were provided on the perforated area. That is why the values of the static pressure on the model surface could only be judged considering the variation of measured static pressure in the upstream and downstream regions of the perforated insert. Those data have shown that, in the indicated regions (except for the vicinities of the leading and trailing edges of the plate), we had a gradient-free flow in which the static pressure could be considered roughly uniform (within the experimental inaccuracy). Additional measurements of mean flow velocity at a height y roughly equal to the height of the outer edge of boundary layer performed with the help of the hot-wire anemometer at fifteen points over the plate length have showed that the maximum difference

$$\Delta U = \left(\frac{U_{\max} - U_{\min}}{U_{\text{aver}}}\right)\cdot 100\ \%$$

never exceeded 0.9 %, where the subscripts “max”, “min”, and “aver” refer, respectively, to the maximum, minimum, and mean flow velocity values. The noted zero-gradient friction was attained due to the installation of the plate at a small (about 10′) positive incidence and due to an adjustment of the flow pattern in the vicinity of the leading edge made with the help of the tail flap.

The local and integral properties of the flow in boundary layer were studied on the basis of measurements of the profiles of mean flow velocity and its instantaneous streamwise fluctuations in some working frequency band and, also, on the basis of surface-friction measurements performed at about twenty cross sections over the length of the model in its central symmetry plane ($z = 0$). The obtained data show that the characteristics of the shear flow on the perforated surface complied with the physical concept of the properties of turbulent boundary layers formed on impermeable smooth flat plates streamlined by gradient-free flows. For instance, the distributions of integral characteristics of the boundary-layer flow

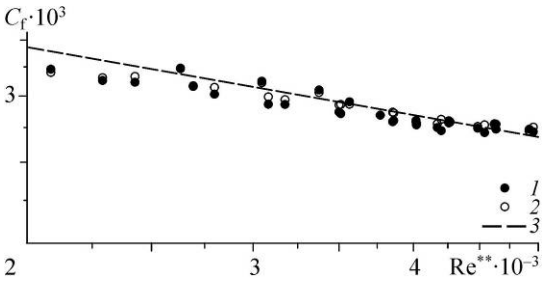

Fig. 2. The skin friction coefficient versus the Reynolds number based on the momentum thickness (in the absence of intake airflow).

1 — logarithmic portion of boundary layer, *2* — data calculated by the procedure proposed by the present authors, *3* —data calculated by formula (2).

such as the displacement thickness δ^* or the momentum thickness δ^{**} exhibited near-standard flow properties.

At the same time, a more representative one is the dependence $C_f = f(\mathrm{Re}^{**})$ (see Fig. 2); this dependence characterizes the variation of the local skin-friction coefficient C_f as a function of Re^{**}, where Re^{**} is the Reynolds number based on the momentum thickness δ^{**}. For comparison, also shown are data calculated by formula [17]

$$C_f = \frac{0.3e^{-1.33H}}{(\lg \mathrm{Re}^{**})^{1.74+0.31H}}, \tag{2}$$

where $H = \delta^*/\delta^{**}$ is the boundary-layer shape factor. Yet, in using formula (2), there arises a question whether the made choice of H is adequate or not. In our opinion, a more substantiated approach consists in the following. It is not the current experimental value of $H(x)$ (leading to a kind of adjustment) but, instead, the value of H in one of the last measured cross sections that was used (in the latter case, the flow was assumed to reach Clauser-equilibrium state). It is the latter constant value that was used in the calculations.

Evidently, on the whole we have quite a satisfactory agreement between the experimental values of C_f and those calculated by formula (2). A more notable difference is observed at low numbers Re^{**}; it seems that this notable difference was due to the fact that, here, the boundary layer had not reached a fully equilibrium state. Yet, the maximum deviation of the experimental values of C_f from the calculated data, including the values obtained on the permeable surface, never exceeded 4 %. The latter result provides direct evidence for the important fact that, in the absence of intake airflow, the flow past the finely perforated wall was almost equivalent to the flow past some analogous hydraulically smooth wall.

The profiles of turbulent velocity fluctuations in boundary layer plotted in the law-of-the-wall variables $\sqrt{\overline{u'^2}}/v_* = f(\lg y^+)$ in the absence of intake airflow have also confirmed the fact that the characteristics of the shear layer on the perforated wall did not contradict the available data on the properties of turbulent boundary layers formed on smooth flat plates under conditions of gradient-free flow.

2.2. Boundary layer in the presence of intake airflow

2.2.1. Motivation

The idea to organize air blowing into boundary layer through an intake with the help of the external pressure flow has arisen in connection with an interesting result that was obtained in our previous study; the essence of the result can be outlined as follows. Among other things, it was found that passive supply of air from atmosphere through the "supply pipelines–pressure chamber–perforated wall" path could be used to reach, under examined conditions, a profound reduction of skin friction on the streamlined surface just due to the natural pressure difference between the barometric and static pressures in the wind-tunnel test section. In the latter case, an increase in freestream velocity leads to a growth of the intensity of the air blowing through perforated wall (this fact is quite natural) and, also, to a related reduction of wall friction.

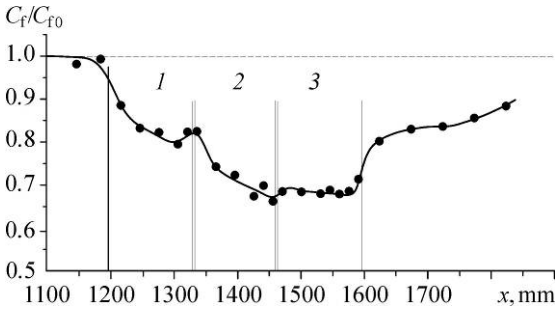

Fig. 3. Distribution of normalized skin friction coefficient over model length. It was obtained under the conditions with the passive overflow due to the natural pressure difference between the barometric and static pressures in the wind-tunnel test section.

As an example, Figure 3 shows measured data on the local values of normalized skin friction coefficient $C_f/C_{f0}(x)$ along the flat plate which were obtained solely due to the above-mentioned passive air overflow. Here, C_{f0} are the values of C_f at the like point at the distance x in the flow without blowing, and $x = x_{eff}$ is the coordinate that characterizes the virtual origin of the turbulent boundary layer. It was found from the condition of coincidence, in the first measurement cross section, of the experimentally found value of δ^{**} and the value of δ^{**} calculated by the procedure developed by Cebeci [18] who used the boundary-layer equations with subsequent upstream calculation till the point x at which $\delta^{**} = 0$; for brevity, in what follows the subscript "eff" will be omitted. In those experiments, the same supply pipelines were used through which traditional (forced) blowing of air out of a pressurized-air line was previously realized [6]. The difference consists in that the blowing region as a whole comprised three isolated permeable surface areas (the boundaries between those surface areas are shown in Fig. 3 with the vertical lines). The rates of the airflows through those surface areas were identical.

Apparently, the passive air overflow, equivalent to some blowing intensity through the finely perforated wall, provides a substantial reduction of skin friction coefficient C_f whose magnitude at the end of the last section exceeds 30 %.

As for the application of the control method under study in practical cases, for instance, at a transport aircraft, this matter calls for an additional thorough analysis. A natural strategy towards implementation of the above approach implies using bypass of air from the cabin, in which life support conditions are produced, through a perforated shell directly overboard. It is apparent, however, that additional supply of energy will then appear necessary for recovery of comfortable on-board conditions, for instance, in terms of pressure. Otherwise, an independent source (say, compressor) for implementing forced blowing will become necessary; of course, this would make the whole aircraft structure heavier. In the last analysis, the efficiency of such a system is to be judged on the basis of the estimated balance between the consumed power and the power gained due to air blowing.

The above results suggest an idea on the necessity to approbate such an approach based on the use of external-flow resources.

2.2.2. The distribution of local and integral characteristics of boundary layer

First of all, we would like to note here that, in principle, the profile of mean velocity in boundary layer in the flow region over the perforated insert in the presence of intake airflow proved to be similar to the profile formed at forced supply of air into the pressure chamber with subsequent uniform blowing of the supplied air into boundary layer [6]. In particular, in the inner region of boundary layer, the distribution of mean velocity in the absence of intake airflow could be rather adequately represented with the classical law-of-the-wall $u^+ = A \log y^+ + B$ (Fig. 4) with the coefficients $A = 5.62$ and $B = 5.0$ [19], where $u^+ = u/v_*$, $y^+ = yv_*/\nu$, and ν is the kinematic viscosity. In the presence of intake airflow, a distinct deviation of the experimental dependence $u^+ = f(y^+)$ from the classical law of the wall was observed. Since the law-of-

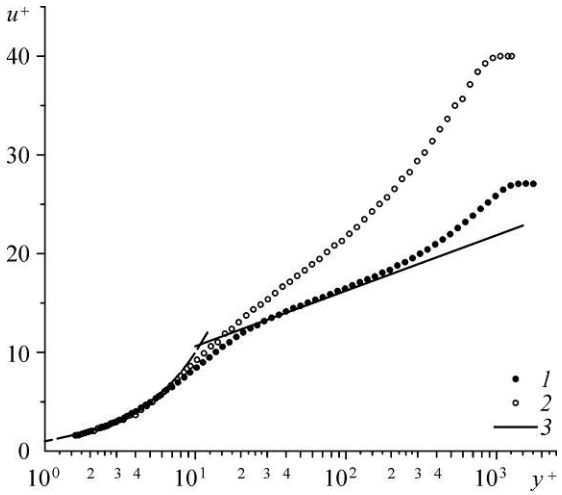

Fig. 4. Mean velocity profiles in law-of-the-wall variables.
Cross section x=1554.3 mm. *1*—with intake airflow, *2*—without intake airflow, *3* — $u^+ = 5.62y^+ + 5$.

the-wall variables, u^+ and y^+, are scaled by dynamic velocity v_*, the latter finding can be regarded as indirect evidence of skin friction reduction. Thus, the same tendency like that in the case of forced air blowing was revealed.

As for the possibility to reproduce the properties of the flow in the outer region of boundary layer, in the present study, like previously, for the check we used an approach that was developed in [20, 21], where for the indicated region the characteristic velocity scale $U_\infty \delta^*/\delta_{99}$ was proposed. It turned out that the experimental velocity profiles $(U_\infty - u)/U_\infty \delta^*/\delta_{99} = f(y/\delta_{99})$ in boundary layer in the region over the permeable plate area normalized using the above velocity scale $U_\infty \delta^*/\delta_{99}$ and obtained in the presence and absence of intake airflow could be generalized, within experimental inaccuracy, with a single dependence. In this sense, those velocity profiles do not contradict the data that were previously obtained for the forced blow of longitudinally uniform blowing intensity.

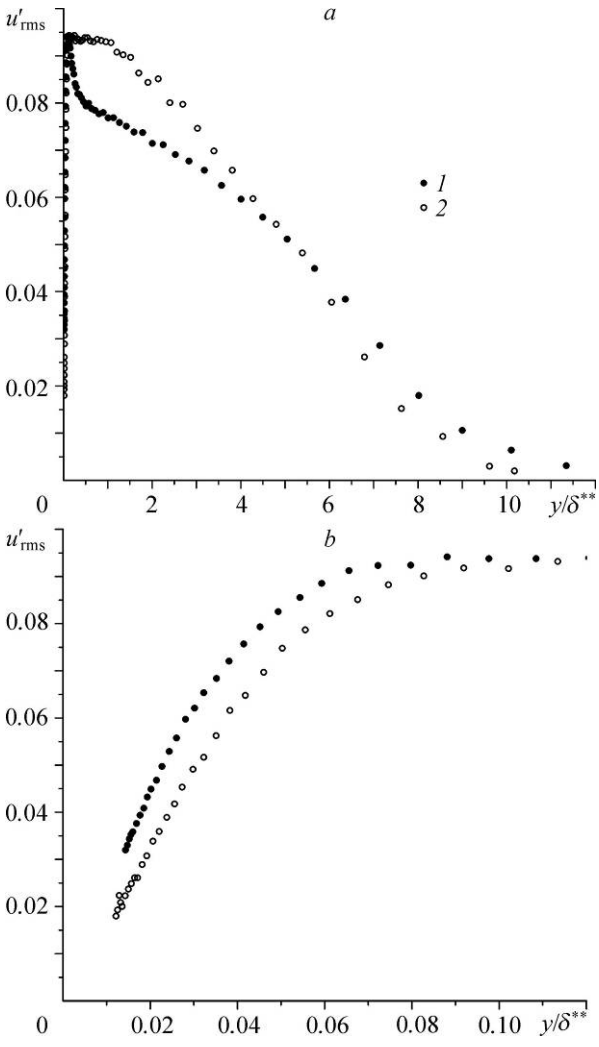

Fig. 5. Streamwise rms velocity fluctuations profiles in the cross section x =1554.3 mm.
1—in the absence of intake airflow, *2*—in the presence of intake airflow.

Consider now the behavior of turbulent velocity fluctuations u'_{rms} in the boundary layer over the perforated plate in the presence of intake airflow. Data reflecting the variation of u'_{rms} are shown in Fig. 5 in the form of the profile $u'_{rms}/U_e = f(y/\delta^{**})$; these data are compared to the similar data obtained in the absence of intake airflow. Over boundary-layer height, three characteristic regions in which the presence of the airflow induces different effects with variation of the coordinate y can be distinguished. In particular, the increased values of u'_{rms} in the region $0.11 \le y/\delta^{**} \le 4.5$

and the decreased values of u'_{rms} in the region $y/\delta^{**} \geq 4.5$ (Fig. 5*a*) in comparison with the case of no intake airflow are noteworthy. Next, consider the flow region immediately adjacent to the wall, $0 \leq y/\delta^{**} \leq 0.11$ (see Fig. 5*b*). Here, decreased values of u'_{rms} are observed as well. The latter observation points to the fact that, in the presence of intake airflow, the maximum of turbulent velocity fluctuations gets forced from the wall, which circumstance is in turn indicative of viscous-sublayer thickening and reduced surface friction. In this respect, here we observe the same tendencies in the variation of flow quantities that are also inherent in the flow in the presence of intake airflow. The only difference consists in that, among the three indicated regions, in the central region, the growth of u'_{rms} extends to larger values of y.

Of particular interest is the efficiency of the control method. In the first approximation, this efficiency can be evaluated on the basis of an experimental and numerical study of the distribution of friction. Figure 6 shows measured data on the normalized values of skin friction coefficient $C_{\mathrm{f}}/C_{\mathrm{f0}}(x)$ (*1*) along the flat plate under conditions with open air intake. The leading and trailing boundaries of the perforated area are shown with dashed vertical lines. For clarity of representation of the friction pattern right in the blowing region and behind it, here the distribution $C_{\mathrm{f}}/C_{\mathrm{f0}}$ in front of the permeable area is represented with few data. Note that the local values of $C_{\mathrm{f}}/C_{\mathrm{f0}}$ in this region are close to the values measured under conditions with plugged air intake. The vertical bars in Fig. 6 show the tripled root-mean-square inaccuracy ($\pm 3\sigma$) of the normalized value of $C_{\mathrm{f}}/C_{\mathrm{f0}}$,

$$\sigma(C_{\mathrm{f}}/C_{\mathrm{f0}}) = \sum_{1}^{n} \frac{[\overline{C_{\mathrm{f}}/C_{\mathrm{f0}}} - (C_{\mathrm{f}}/C_{\mathrm{f0}})_i]^2}{n-1},$$

determined from repeated measurements of this quantity in one and the same cross section performed under conditions with open air intake. Here, $n = 7$ is the number of measurements, $\overline{C_{\mathrm{f}}/C_{\mathrm{f0}}}$ is the arithmetical mean value, and $(C_{\mathrm{f}}/C_{\mathrm{f0}})_i$ is the *i*th value of measured data.

Evidently, the error in determining the skin friction coefficient value is rather large. This large error is due to the formation of an unsteady flow pattern in the intake channel. We failed to identify the actual reason for this phenomenon since subtle measurements in the channel itself were hard to perform because of limited access. Probably, the emergence of nonstationarity is related to the formation of eddies in the rear part of the intake and, also, behind the technological ledge; the latter is confirmed by the calculated data on the flow pattern in intake channel shown in Fig. 7 (note that, here, the linear scales along the *x*- and *y*-axes are different). Obviously, the mentioned eddies and the related flow oscillations in intake channel could induce additional perturbations into boundary layer on the surface of the perforated insert; it is the latter factor that has led to the scatter of mean flow velocity values measured

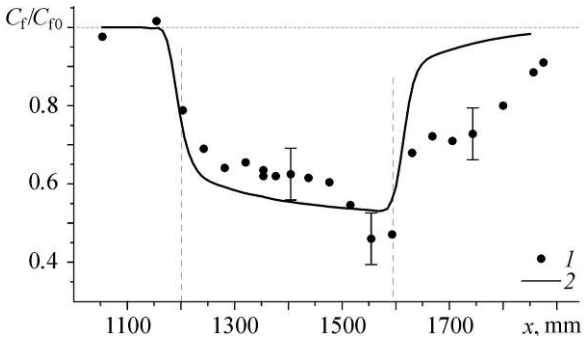

Fig. 6. Distribution of the normalized skin friction coefficient over the length of the model.
1 — experimental data, *2* — calculated data.

in the near-wall zone of the flow and to the related increase of the error in determining the value of C_f/C_{f0}. Anyway, it is quite apparent that in the future experiments, the intake channel configuration needs to be modernized.

At the present state of the study, a more important one is the substantial reduction of skin friction coefficient in the presence of intake airflow (see Fig. 6). Yet, the rate of change of the value of C_f/C_{f0} is far from being uniform over the plate length. The most pronounced reduction of friction can be achieved at the end of the perforated insert, where the difference from the non-modified flow, determined as $\Delta C_f/C_{f0}$, reaches a value of order 50 %. For comparison, the same figure shows numerical data on skin friction coefficient (*2*) obtained using the Reynolds-averaged Navier–Stokes equations and the differential two-parametric k-ε model. Strictly speaking, such a problem is to be solved in 3D statement, which requires considerable computational resources. That is why, as was noted above, at the present stage of the study, the calculations were carried out using a simplified approach, that is, in the 2D approximation in which the perforated surface was replaced with a surface with slits. Nonetheless, it is seen that, on the whole, the calculated data, at least in the region over the perforated surface, rather adequately reflect the behavior of C_f/C_{f0}. At the same time, some features of the flow at the interface between the permeable and impermeable surface areas and behind this interface (see below) hamper the obtaining of an adequate solution in this flow region; this circumstance is evident from the substantial difference between the experimental and calculated data. Apparently, further progress along this line can be achieved via development of advanced algorithms for calculating the flow of interest with allowance for all revealed features.

Indeed, it also follows from Fig. 6 that the region with the reduced values of C_f/C_{f0} covers not only the perforated surface; it also develops in downstream direction over the impermeable part of the plate. In the region right behind the perforated insert, the skin friction coefficient increases sharply; however, with further increase of x ($x > 1640$ mm), the rate of growth of C_f/C_{f0} substantially decreases. Evidently, in this region, the value of C_f/C_{f0} does not return (at least, in a jumping manner) to the magnitude typical of the state of the flow under conditions with closed air intake. It is important to note that the region with reduced friction values is rather an extended one, stretching in downstream direction over a distance not shorter than half the length of the permeable insert.

The non-asymptotic behavior of C_f/C_{f0} behind the blowing region is hard to attribute just to the sharp change of flow conditions at the interface between the permeable and impermeable surface areas. If this were the case, it could then be expected that the reaction of the flow to a change of boundary conditions would manifest itself as a slow relaxation of main flow quantities (including the friction) to the state of full hydrodynamic equilibrium [22]. However,

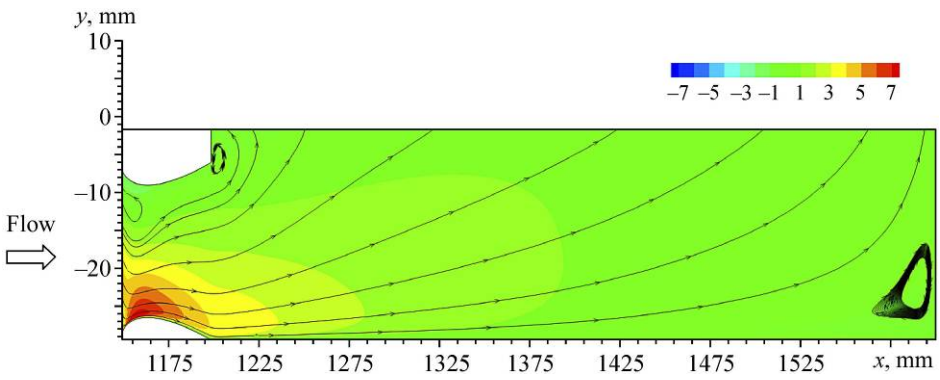

Fig. 7. Numerical data for the flow in the air intake with intake airflow.
The color grade characterizes flow regions with different flow velocities, m/s; the arrows are the velocity vectors.

this is not the case, like it was in the case of forced supply of air through an intermediate pressure chamber [6]. That is why, in our opinion, the most likely one is the following interpretation of the dependence $C_f/C_{f0} = C_f/C_{f0}(x)$ in the mentioned flow region. Under the examined conditions, the wall-normal local flow velocity, amounting to several tenth fractions of percent of freestream velocity U_∞ is small. Simultaneously, the overall effect due to the natural thickening of boundary layer in the direction of x and due to blowing can be expected to promote the turning of the velocity vector over the perforated surface in external-flow direction. As the shear flow reaches the interface between the permeable and impermeable surface areas, the wall-normal velocity vanishes, and this leads to a breakdown of the flow with the formation of a roll eddy with angular rotation velocity ω_z. This in turn promotes a decrease of the growth rate of surface friction in a restricted flow region behind the perforated wall. Since there exist no sources for input of energy into the eddy, then, with increase of longitudinal coordinate x, the eddy decays and, finally, dissipates completely. As a consequence, the coefficient C_f gradually reaches a value close to the equilibrium one.

Also, it should be noted that the above-indicated flow region with reduced friction values behind the active blowing region is of substantial importance for the balance of the net aerodynamic drag of the whole plate/intake combination. Indeed, the drag coefficient C_x of the examined configuration is the sum of the external drag coefficient C_{xw}, defined by the momentum loss in boundary layer; the internal drag coefficient ΔC_x, equivalent to the power spent on the blowing process; the drag coefficient of the air intake itself $C_{x\text{inl}}$; and the interference component $\Delta C_{x\text{int}}$ of the plate/air intake combination:

$$C_x = C_{xw} + \Delta C_x + C_{x\text{inl}} + \Delta C_{x\text{int}}. \tag{3}$$

Since the first drag component is determined by integrating the dependence $C_f = f(x)$ along the plate, including the flow region behind the perforated sample, it is clear that the latter fact will result in an additional gain in drag. Because of the large extension of the indicated relaxation region, the net gain in C_x may appear substantial. Determination of the first and second drag components presents no difficulty. As for the third component and, especially, the contribution to the total drag due to the fourth component (plate/air intake interference), at the present stage of the study, the determination of those components presents too difficult a task. That is why in future experiments, with the aim to measure the overall aerodynamic drag of the model configuration with operating air intake, we are going to implement the weighing technique. This will permit evaluation of the net effectiveness of this device as a means to control the turbulent boundary layer by the analyzed method. The evaluation procedure can be developed based on the use of a "floating" element presenting an area "cut out" from the streamlined surface. The difficulty here consists in that such an area has to include not only the perforated insert itself and an air intake suspended underneath the insert but, also, an extended portion of the surrounding flat-plate surface since, as was shown above, the downstream region with a pronounced effect due to blowing and air intake is quite considerable.

In conclusion, we would like to emphasize that the mechanism of friction reduction on the perforated surface is identified quite reliably. The presence of intake airflow and the action of blowing on the wall flow promote an increase of laminar-sublayer thickness in the turbulent boundary layer over the streamlined surface (Fig. 8). As a result, the local velocity in the vicinity of the wall decreases, thus reducing the friction. We would like to note that rather large a scatter of the values of δ_L seems to be due to the same reason.

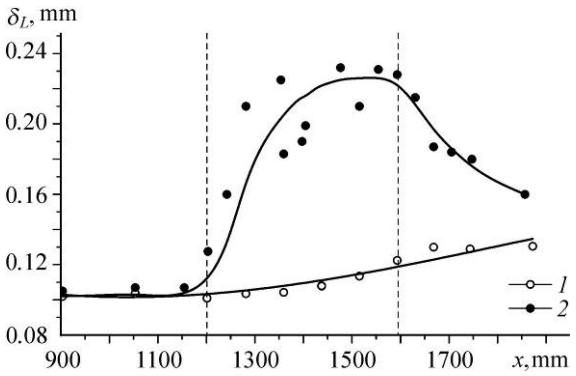

Fig. 8. Variation of laminar-sublayer thickness over the length of the model.
1 — without intake airflow,
2 — with intake airflow.

Conclusions

The results of the present numerical and experimental study aimed at investigation of the possibility of skin friction reduction in incompressible turbulent flat-plate boundary layer via air blowing through a finely perforated wall organized due to the supply of external-pressure-flow air through an intake installed on the idle part of the model allow the following conclusions to be drawn.

1. Passive air blowing through a finely perforated wall due to external-pressure-flow resources offers quite efficient a means to exert an action on turbulent boundary layer. Under the examined conditions, such an approach has proved capable of ensuring a stable reduction of the local values of skin friction coefficient C_f over the model length reaching 50 % at the end of the perforated insert. There still remains a reserve for further reduction of C_f due to the application of an intake with an improved flow-channel configuration and, possibly, due to optimized location of the intake over height in boundary layer.

2. A final conclusion on the aerodynamic efficiency of the proposed method to control the turbulent boundary layer can be made considering measured data on the net aerodynamic drag of the flat plate/channeled intake combination. Such studies based on the use of the weighing technique should become a subject of further study.

3. Numerical data characterizing the variation of local characteristics in the blowing-modified turbulent boundary layer over a perforated surface (in particular, skin friction) rather adequately reproduce the tendencies exhibited by the experimental data. At the same time, further advancements in solving the problem are only possible on the development of improved algorithms and numerical methods for calculating the flow of interest.

References

1. **R. Wood,** Impact of advanced aerodynamic technology on transportation energy consumption, SAE International TP-2004-01-1306, 2004, 21 p.
2. **A. Abbas, J. de Vicente, and E. Valero,** Aerodynamic technologies to improve aircraft performance, Aerospace Science and Technology, 2013, Vol. 28, P. 100–132.
3. **D.P. Hwang,** A proof of concept experiment for reducing skin friction by using a micro-blowing technique, AIAA Paper, 1997, No. 97–0546 (NASA TM-107315).
4. **D.P. Hwang,** Review of research into the concept of the microblowing technique for turbulent skin friction reduction, Progress in Aerospace Sci., 2004, Vol. 40, P. 559–575.
5. **T.G. Tillman and D.P. Hwang,** Drag reduction on a large-scale nacelle using a microblowing technique, 37th AIAA Aerospace Sci. Meeting and Exhibit, Reno, NV, January 1999, AIAA Paper No. 1999–0130.
6. **V.I. Kornilov and A.V. Boiko,** Efficiency of air microblowing through microperforated wall for flat plate drag reduction, AIAA J., 2012, Vol. 50, No. 3, P. 724–732.
7. **Y.L. Lin, M.K. Chyu, T.I.P. Shih, B.P. Willis, and D.P. Hwang,** Skin friction reduction through micro blowing, AIAA Paper, 1998, No. 98–0359.
8. **J. Li, C.-H. Lee, L. Jia, and X. Li,** Numerical study on the flow control by micro-blowing, 47th AIAA Aerospace Sciences Meeting, Orlando, Fl., January 2009, AIAA Paper, No. 2009–779.
9. **V.I. Kornilov, I.N. Kavun, and A.N. Popkov,** Application of a cascade method to control turbulent boundary layer with blowing, Vestnik NGU, Ser. Fizika, 2014, Vol. 9, Iss. 1, P. 49–61.
10. **D.P. Hwang,** Experimental study of characteristics of micro-hole porous skins for turbulent skin friction reduction, in: I. Grant (Ed.) Proc. 23rd Cong. Int. Council of the Aeronautical Sci., Toronto, Canada: Optimage Ltd., 2002, P. 2101.1–2101.7.

11. A.V. Bazovkin, V.M. Kovenya, V.I. Kornilov, A.S. Lebedev, and A.N. Popkov, Effect of micro-blowing of a gas from the surface of a flat plate on its drag, J. Appl. Mech. Techn. Phys., 2012, Vol. 53, No. 4, P. 490–499.
12. S.S. Kutateladze and A.I. Leont'ev, Heat Transfer, Mass Transfer, and Friction in Turbulent Boundary Layer, Hemisphere Publishing Corporation, New York, Washington, Philadelphia, London, 1990.
13. V.I. Kornilov, Three-Dimensional Near-Wall Turbulent Flows in Corner Configurations, 2nd edition, Russian Academy of Sciences, Siberian Division, Novosibirsk, 2013.
14. A.V. Boiko and V.I. Kornilov, Hot-wire anemometer measurement of local skin friction coefficient, Thermophysics and Aeromechanics, 2010, Vol. 17, No. 4, P. 577–586.
15. P.S. Klebanoff, Characteristics of turbulence in a boundary layer with zero pressure gradient, NACA Rept. 1247, 1955, P. 1135–1153.
16. B.E. Launder and D.B. Spalding, Lectures in Mathematical Models of Turbulence, Academic Press, London, New York, 1972.
17. F.M. White, Viscous Fluid Flow, 2nd edition, McGraw-Hill, New York, 1991.
18. T. Cebeci, Analysis of Turbulent Flows, Elsevier Ltd, Oxford, 2004.
19. Computation of Turbulent Boundary Layer, in: Proc. Stanford Conf. AFOSR-IFP, 1968–1969, Eds. D.E. Coles and E.A. Hirst, Stanford University, 1969, Vol. 2.
20. M.V. Zagarola and A.J. Smits, A new mean velocity scaling for turbulent boundary layers, in: Proc. 1998 ASME Fluids Engng Division Summer Meeting, June 21–25, Washington DC, 1998, P. 1–6.
21. R.B. Cal and L. Castillo, Similarity analysis for transpired turbulent boundary layers subjected to external pressure gradients, AIAA J., 2005, Vol. 43, No. 9, P. 1913–1922.
22. J.F. Nash, Turbulent boundary layer behavior and the auxiliary equation, NPL Aeron. Rep., 1965, No. 1137.